

# Multicharged Supramolecular Assembly Mediated by Polycationic Cyclodextrin for Efficiently Photodynamic Antibacteria

Xianyin Dai, Bing Zhang, Qilin Yu, and Yu Liu\*

Cite This: <https://doi.org/10.1021/acsabm.1c01018>

Read Online

ACCESS |



Metrics &amp; More



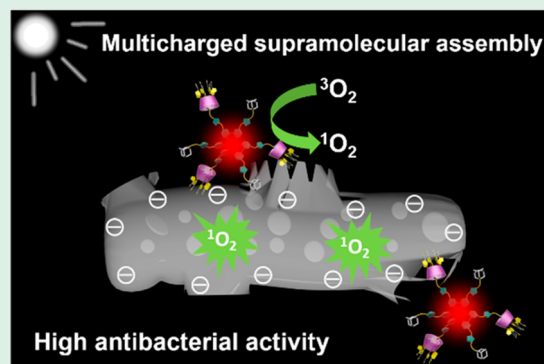
Article Recommendations



Supporting Information

**ABSTRACT:** Supramolecular antimicrobial materials based on synthetic macrocycles have recently aroused enormous interests due to their controllable and effective antibacterial treatment. Herein, a multicharged supramolecular assembly was fabricated employing the moderate host–guest interaction between hexa-adamantane-appended ruthenium polypyridyl (Ru2) and polycationic cyclodextrin (CD-QAS) in water. The positively multicharged feature of supramolecular assembly could remarkably enhance the specific intercalation and accumulation in negatively charged bacteria membrane leading to the physical membrane damage. Subsequently, the assembly could efficiently initiate the significant generation of singlet oxygen ( $^1\text{O}_2$ ) in situ when irradiated with white light thus exhibiting a highly efficient antibacterial capability. Significantly, antibacterial experiments indicated that Ru2/CD-QAS displayed less effect on suppressing the growth of *E. coli* only about 25% in the absence of light while they exhibited excellent killing efficiency more than 99% toward *E. coli* under light irradiation. This work provides a simple approach for constructing supramolecular antimicrobial materials for synergistic photodynamic antibacteria.

**KEYWORDS:** polycationic cyclodextrin, host–guest interaction, multicharged supramolecular assembly, bacterial membrane intercalation, photodynamic antibacteria



## INTRODUCTION

In the past decades, bacterial infections have been serious global health concerns because of high morbidities and mortalities.<sup>1</sup> Antibiotics have played major roles in combating pathogenic microbes and contributed enormously to human health. However, a growing number of bacteria are becoming antibiotic resistance because of the misuse and overuse of antibiotics, which brings a considerable degree of difficulty to the antimicrobial therapy.<sup>2,3</sup> Hence, it is of great importance to search for smart strategies against these dangerous pathogenic bacteria. Cationic quaternary ammonium compounds and cationic polymers like polyethylenimine derivatives, chitosan, and  $\epsilon$ -poly-L-lysine which were equipped with large numbers of positively charged sites have been widely developed as biomaterials against pathogens on account of their remarkably broad-spectrum antibacterial effect.<sup>4–9</sup> Moreover, photodynamic therapy (PDT) has evolved as an alternative method to combat microbial infections,<sup>10–12</sup> which exhibits several merits such as minimal invasiveness, spatiotemporal selectivity, and notably no multidrug resistance. Specifically, this therapy relies mainly on the excited state photosensitizers to produce highly cytotoxic reactive oxygen species (ROS) when activated by light.<sup>13,14</sup> Subsequently ROS can rapidly suppress the activity of the enzyme then ultimately trigger cell necrosis or apoptosis. In this regard, combining cationic pendant groups and

photosensitizers into the design antibacterial material is a promising approach for improving the antibacterial efficiency considering the short half-life (<40 ns) and limited action radius (<20 nm) of  $^1\text{O}_2$ .<sup>15,16</sup> Additionally, Gram-negative bacteria were insensitive to  $^1\text{O}_2$  because of its complicated cell membrane with limited permeability and extra defense mechanisms by contrast with Gram-positive bacteria, which makes it difficult for  $^1\text{O}_2$  diffusion to kill bacteria.<sup>17,18</sup> Although numerous antibacterial agents such as conjugated polymers and conjugated oligoelectrolytes have been successfully applied to photodynamic killing bacteria with effective antibacterial activity,<sup>19,20</sup> these antibacterial materials generally composed of cationic pendant groups for insertion into a negative-charged bacteria membrane and  $\pi$ -conjugated backbone structure for producing ROS primarily relied on the covalent interactions, the majority of which usually include an elaborate synthesis procedure and complicated purification during the construction process of antibacterial materials. Therefore,

**Received:** September 21, 2021

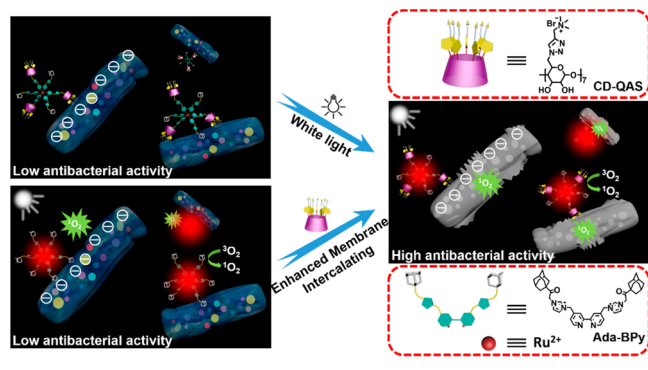
**Accepted:** November 2, 2021

finding an efficient and convenient approach toward the construction of antibacterial materials is highly desirable.

Supramolecular chemistry which mainly focused on the noncovalent interactions has offered an alternative method for fabricating complicated molecular assemblies expediently through host–guest recognition.<sup>21,22</sup> Supramolecular antimicrobial materials based on macrocyclic compounds are the current hot spot for effective antibacterial treatment.<sup>23</sup> Moreover, the constructed supramolecular assembly exhibited reversibility and adaptive capability when in contact with external stimuli due to the dynamic interaction, which can precisely regulate their biological actions on demand.<sup>24</sup> Recently, Yang and Gao et al. constructed a robust antibacterial system utilizing cationic polyaspartamide and anionic carboxylatopillar[5]arene via host–guest interactions between the quaternary ammonium attached to polyaspartamide and CP[5]A, revealing an enhanced biocompatibility and selective antibacterial activity.<sup>25</sup> Wang et al. reported a novel guanidinium-modified pillar[5]arene which could efficiently penetrate through biofilm barriers and simultaneously accommodated a conventional antibiotic cefazolin sodium thus realizing high antibacterial potency.<sup>26</sup> Our group also fabricated a supramolecular hydrogel consisting of chitosan modified with  $\beta$ -cyclodextrin and anionic drug diclofenac sodium as well as  $\text{AgNO}_3$  for efficient bacterial infection treatment.<sup>27</sup>

Having these considerations, we herein presented a antibacterial system using the noncovalent supramolecular complexation of hexa-adamantane-appended ruthenium polypyridyl (Ru2) and polycationic cyclodextrin (CD-QAS) and investigated its potential abilities for combatting bacteria (Scheme 1). There were some inherent advantages for this

**Scheme 1. Schematic Representation of the Multicharged Supramolecular Assembly with Chemical Structures of the Host and Guest Molecule and Its Efficient Photodynamic Antibacterial Therapy**



constructed system: (1) CD-QAS as a positively charged macrocyclic receptor possessing favorable water-solubility, low toxicity and superior biocompatibility, more importantly, could tightly bind and accumulate in the bacteria negatively charged membrane;<sup>28–30</sup> (2) the adamantane appended Ru1 and Ru2 not only had favorable water solubility and long fluorescence emission, but also could generate ROS efficiently in the presence of light; (3) the multicharged supramolecular assembly simply fabricated profiting from strong host–guest interaction between adamantane and CD-QAS could achieve effective membrane accumulation and  $^1\text{O}_2$  generation in situ simultaneously, thereby killing bacteria efficiently. Conse-

quently, the obtained supramolecular assembly might offer a new approach for the design of new antibacterial material.

## RESULTS AND DISCUSSION

Details on the synthesis of Ru1, Ru2, and CD-QAS are presented in Schemes S1 and S2 and fully characterized by  $^1\text{H}$ ,  $^{13}\text{C}$  NMR, IR, and ESI-MS spectroscopy (Figures S1–S6). First, the photophysical properties of Ru1 and Ru2 were evaluated in aqueous solution. Ru1 and Ru2 all exhibited the maximum absorption peak centered on 285 nm, which derived from the characteristic  $\pi$ – $\pi^*$  intraligand transitions assigned to the adamantane-modified bipyridine imidazolium (Ada-Bpy). Meanwhile, another typical metal-to-ligand charge-transfer (MLCT) transitions absorption band of the Ru(II) center was observed in the range from 400 to 550 nm in the visible region (Figure S7a,c). The fluorescence emission spectra of Ru1 and Ru2 showed a maximum peak at around 630 and 650 nm, respectively, which mainly relied on the MLCT based emission (Figure S7b,d). Such similar spectra implied that their spectra primarily depended on the Ru(II) center. Additionally, the absorption and emission peaks of Ru1 and Ru2 were found to be barely changing after adding the corresponding equivalent CD-QAS. These results illustrated that the complexation with CD-QAS did not affect the photophysical properties of the Ru(II) center.

To explore the noncovalent interaction between the complex and CD-QAS, Ada-Bpy was employed as a reference guest for  $^1\text{H}$  NMR titration. Job analysis showed that the binding stoichiometry of them was 1:1 in which a molar fraction of 0.5 was observed at the maximum as indicated in Figure 1d. Other than that, when CD-QAS was gradually added into Ada-Bpy, the adamantyl protons all displayed downfield shifts with shape changes, illustrating inclusion of the adamantane in the CD-QAS cavity (Figure 1a). The binding constant ( $K_s$ ) of Ada-Bpy with CD-QAS was determined as  $1.2 \times 10^3 \text{ M}^{-1}$  according to the nonlinear least-squares fit of the titration data (Figure 1b). Subsequently, the binding behaviors between Ru2 (or Ru1) and CD-QAS were further confirmed. The proton signals of adamantane (Ha–c) all showed a significant downfield shift in the presence of CD-QAS (Figures 1c and S8), which definitely demonstrated that the Ada moiety penetrated into the CD-QAS cavity. The possible pattern of such assembly was shown in Scheme 1.

After successful construction of the supramolecular assembly, an agarose gel electrophoresis experiment was carried out to study the DNA photocleavage ability and condensation behavior with pBR322 plasmid DNA as a model substrate in the presence or absence of the supramolecular assembly. Ru1/CD-QAS assembly exhibited a concentration-dependent photoinduced DNA cleavage ability, and close supercoiled DNA (form I) was gradually resolved into nicked circular DNA (form II) under light irradiation for 1 min (Figure S9). In contrast, the pBR322 plasmid DNA alone exhibited no obvious DNA cleavage with light. Moreover, the DNA photocleavage and condensation ability of Ru2/CD-QAS assembly could be observed at the same time with the increase of the concentration. When the concentration of Ru2 in the assembly was up to  $4 \mu\text{M}$ , the pBR322 plasmid DNA could be completely condensed and cleaved into nicked DNA (form II) under white light irradiation. The different effects of these two assemblies on pBR322 plasmid DNA might be mainly due to the difference in generation ROS ability of Ru1 and Ru2 and

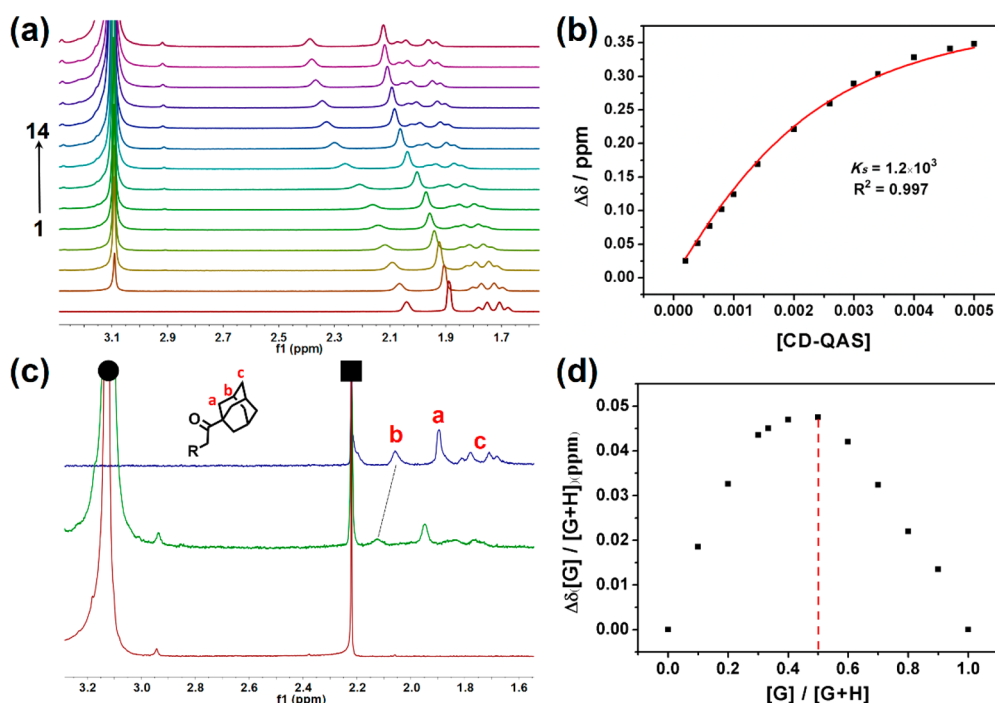


**Figure 1.**  $^1\text{H}$  NMR titration of Ada-Bpy with CD-QAS. (a)  $^1\text{H}$  NMR spectra of Ada-Bpy (1 mM) with addition of 0, 0.2, 0.4, 0.6, 0.8, 1.0, 1.4, 2.0, 2.6, 3.0, 3.4, 4.0, 4.6, and 5.0 mM CD-QAS (spectra from 1 to 14) in  $\text{D}_2\text{O}$  at  $25^\circ\text{C}$ . (b) Nonlinear least-squares fit of the chemical shift changes of the Ada-Bpy peaks at  $d = 2.03$  ppm as a function of the concentration of CD-QAS. (c) Partial  $^1\text{H}$  NMR spectra of free Ru2 (blue line), the Ru2/CD-QAS complex (green line), and free CD-QAS (red line) in  $\text{D}_2\text{O}$  ( $[\text{Ru}2] = 0.1$  mM,  $[\text{CD-QAS}] = 0.3$  mM). Acetone was added as an external reference. The acetone was denoted as symbols ■. (d) The Job's plot of Ada-Bpy (G) and [CD-QAS] (H) in  $\text{D}_2\text{O}$  ( $[\text{Ada-Bpy}] + [\text{CD-QAS}] = 1$  mM) at  $25^\circ\text{C}$ .

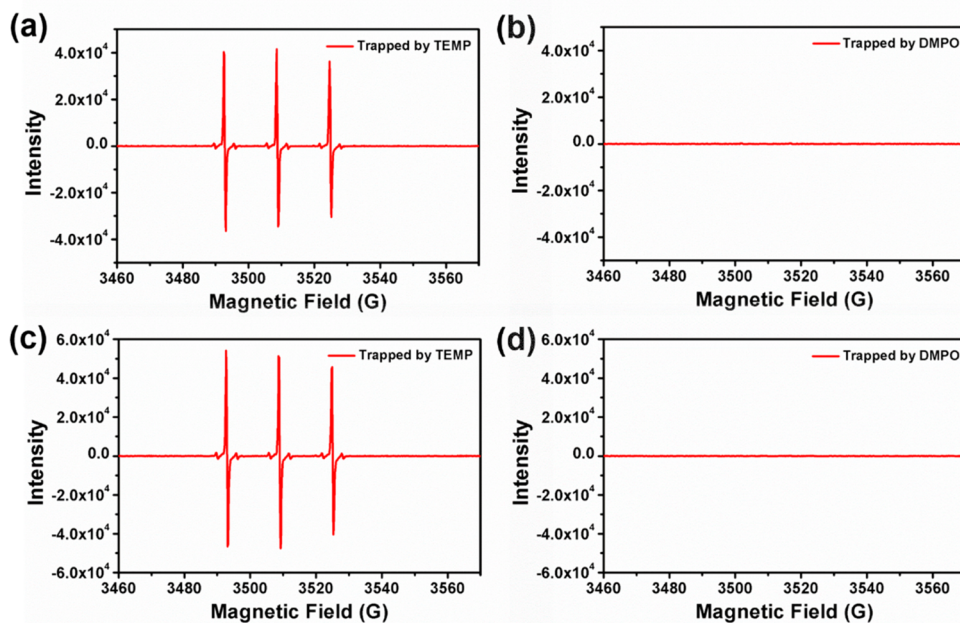


**Figure 2.** Electron spin resonance (ESR) spectra of Ru1 (a and b) and Ru2 (c and d; both at 0.1 mM) detected with TEMP and DMPO as the spin-trap in water.

the number of charges carried by the assemblies. Therefore, these assemblies might be potentially applicable in photodynamic therapy.

It was well-known that there were two types of mechanisms for ROS generation including the hydroxyl radical ( $\bullet\text{OH}$ ) and  $^1\text{O}_2$  which was respectively produced via the type I mechanism

and type II mechanism.<sup>31</sup> To estimate the mechanism of ROS generation, electron spin resonance (ESR) experiments were utilized to monitor the different types of ROS production with TEMP or DMPO as the trapping agents to confirm the  $^1\text{O}_2$  and  $\bullet\text{OH}$  formation. As revealed in Figure 2, after white light irradiation for 10 min a characteristic three-line signal resulting

from the TEMP- $^1\text{O}_2$  adduct with 1:1:1 intensity ratio was found in the ESR spectrum of both Ru1 and Ru2. In contrast, Ru1 and Ru2 did not promote any  $\bullet\text{OH}$  formation when using DMPO as a probe. These results jointly suggested that the Ru1 and Ru2 could be employed as an efficient  $^1\text{O}_2$  creator via the type II mechanism. Next, 9,10-anthracenediylbis(methylene)-dimalonic acid (ABDA), a common detecting agent for  $^1\text{O}_2$ , was chosen to assess the  $^1\text{O}_2$  generation ability of Ru1 and Ru2 under white light irradiation. The measurement mechanism of ABDA for detecting  $^1\text{O}_2$  was shown in Figure S10. ABDA could selectively capture the  $^1\text{O}_2$  produced in solution, resulting in a decrease in absorption. We utilized the directly purchased  $[\text{Ru}(\text{bpy})_3]\text{Cl}_2$  as a standard to illustrate such unique properties of Ru1 and Ru2. Compared with  $[\text{Ru}(\text{bpy})_3]\text{Cl}_2$ , the absorption peaks of ABDA mixed with Ru1 and Ru2 decreased faster significantly, which meant that they exhibited higher efficiency to produce  $^1\text{O}_2$  (Figure S11). Furthermore, Ru2 presented the most effective  $^1\text{O}_2$  generation ability in water. The  $^1\text{O}_2$  generation quantum yields for Ru1 and Ru2 under light irradiation were evaluated by comparison with  $[\text{Ru}(\text{bpy})_3]\text{Cl}_2$  whose  $^1\text{O}_2$  generation quantum yield was 0.18 in  $\text{H}_2\text{O}$ ,<sup>32</sup> which were calculated as 0.29 and 0.81, respectively (Figure S12).

Subsequently, *E. coli* were used as a Gram-negative bacteria model to assess the photodynamic antibacterial activity of different samples in vitro by using the propidium iodide (PI)-staining method. The living *E. coli* would prevent PI from entering the cell because the cell membrane was intact. However, the cell membrane of dead *E. coli* was damaged, and PI would enter into it to interact with DNA. So PI could selectively detect the death of the *E. coli*. First, the antibacterial efficiency of CD-QAS was tested. As the results shown in Figure 3a, the bacteria in control and CD-QAS groups showed negligible agglomeration or PI emission. In other words, *E. coli* exhibited high viability after treatment with CD-QAS before and after light irradiation, demonstrating no obvious cytotoxicity of the polycationic cyclodextrin at this concentration. Moreover, CD-QAS displayed obvious dose-dependent

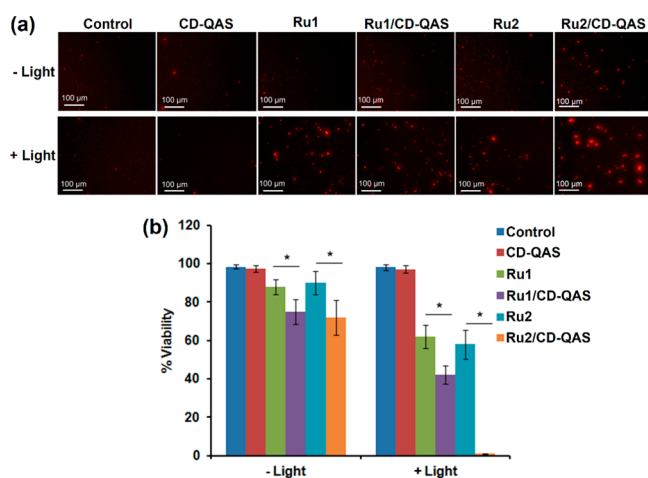


**Figure 3.** (a) Fluorescence images of *E. coli* incubated with different samples for 10 min followed by white light exposure for 10 min and staining with 1.5  $\mu\text{M}$  PI for 10 min. (b) Killing efficiency of different samples on *E. coli* in the absence and presence of white light irradiation for 10 min. Error bars represent the standard deviation of the mean ( $n = 3$ ). \* indicates a significant difference between the control group and the treated group ( $P < 0.05$ ).

antimicrobial activity under the same experimental condition where the bacteriostatic rate was more than 90% when the concentration of CD-QAS was up to 0.9 mM (Figure S13). In addition, light irradiation alone also showed no obvious antibacterial effect. The cell survival rates of Ru1 and Ru2 were 62% and 58%, respectively. Additionally, Ru1 and Ru2 displayed negligible antibacterial effect with the high viability (over 90%) in the dark as revealed by the fluorescence images. The supramolecular assembly Ru1/CD-QAS exhibited high killing efficiency (58%) toward *E. coli* under light irradiation for 10 min, while killing efficiency less than 25% was obtained in the absence of light as indicated in Figure 3b. Furthermore, *E. coli* were killed more than 99% by Ru2/CD-QAS assembly under light conditions, while without light irradiation they showed less effect on suppressing the growth of *E. coli* to only about 25%. As depicted in Figure 3a, significant bacterial accumulation with bright red fluorescence was observed when the *E. coli* were treated with Ru2/CD-QAS assembly under light irradiation for 10 min, indicating that this assembly could be as an efficient agent to remarkably inhibit the growth of *E. coli*. Importantly, the Ru2/CD-QAS showed higher antibacterial activity than Ru1/CD-QAS under the same experimental conditions which was mainly due to the more effective  $^1\text{O}_2$  generation ability of Ru2 and more positive charge within Ru2/CD-QAS assembly. All these results indicated that Ru1/CD-QAS and Ru2/CD-QAS showed much higher antibacterial activity than Ru1 and Ru2 alone benefiting from the multivalent synergistic host-guest interactions between CD-QAS and multiple binding sites supplied by photosensitizers which also ensured the relative stability of the assembly during antibacterial process. Therefore, the introduction of CD-QAS to this supramolecular assembly could significantly enhance the interaction with bacterial cell membranes; thus, the generation of  $^1\text{O}_2$  under light caused a stronger killing effect on bacteria. In addition, the cytotoxicity of these supramolecular systems against 293T normal cells were evaluated. As shown in Figure S14, Ru1/CD-QAS or Ru2/CD-QAS showed little cytotoxicity toward 293T normal cells in the absence of light, indicating their favorable biocompatibility.

To investigate the antibacterial mechanism of Ru2/CD-QAS assembly, *E. coli* cells stained with the assembly were observed by confocal laser scanning microscopy (CLSM). DAPI (4', 6-diamidino-2-phenylindole) was employed to stain the nucleus of the cells. As could be seen in Figure 4, red halo patterns

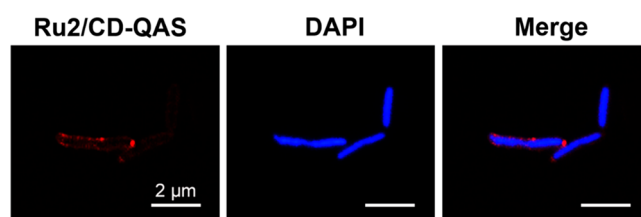


**Figure 4.** CLSM images of *E. coli* incubated with Ru2/CD-QAS assembly for 1 h. The colors of DAPI and assembly are blue and red, respectively. Scale bars are 2  $\mu\text{m}$ .

from assembly were visually distinguished on the periphery of the cells, while bright blue fluorescence from DAPI could be clearly observed in the interior of the cells. These phenomena jointly indicated that the DAPI were mainly located inside the cells, whereas the assembly was preferentially distributed in the

outer portion of the cells due to the enhanced membrane intercalation, leading to the promotion of bacteria death.

Scanning electron microscopy (SEM) studies were also conducted to visualize the morphology changes of *E. coli* cells when treated by the Ru2/CD-QAS assembly. It could be observed that the bacterial cells only under white light still grew in good condition and remained regular with surface integrity and smooth bodies as well as the control group, illustrating that the white light alone did not have any effect on bacteria (Figure 5a,b). However, the bacterial cells membrane

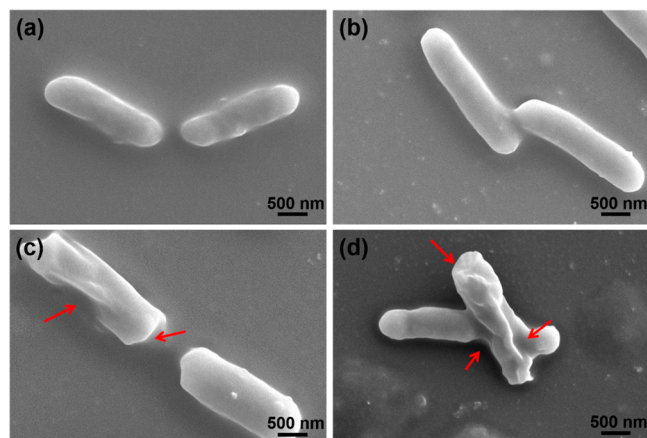


**Figure 5.** Morphology of (a) *E. coli* without Ru2/CD-QAS and light under SEM images; (b) *E. coli* with light but without Ru2/CD-QAS; (c) *E. coli* with Ru2/CD-QAS but without light; and (d) *E. coli* with Ru2/CD-QAS and light. The red arrows suggest the collapse and fusion of membranes.

slightly collapsed and split with the treatment of Ru2/CD-QAS assembly owing to the insertion of quaternary ammonium groups into the negatively charged bacteria membrane (Figure 5c). Furthermore, quite significant changes happened on *E. coli* cells under white light irradiation, whose membrane morphologies were severely collapsed, shrunken, and fused (Figure 5d). The SEM results convincingly proved that the presence of multicharged Ru2/CD-QAS assembly and white light irradiation together could result in severe bacterial death efficiently revealed by the morphology changes.

## CONCLUSIONS

In summary, we synthesized two types of red fluorescence adamantane-modified ruthenium polypyridyls (Ru1 and Ru2) as photosensitizers, and Ru2 possessed better  $^1\text{O}_2$  generation ability in aqueous solution. Profiting from the highly noncovalent binding, a positively multicharged antibacterial supramolecular assembly was simply fabricated using CD-QAS and Ru2. Antimicrobial experiments demonstrated that this assembly displayed the most effective antimicrobial performance for Gram-negative bacteria *E. coli* under light in comparison with Ru1/CD-QAS. Additionally, the sole Ru2 under white light and Ru2/CD-QAS without light irradiation all displayed a relatively low antimicrobial effect, so the antimicrobial activity could be regulated in a controlled manner. Based on CLSM and SEM studies, the excellent bactericidal activity of Ru2/CD-QAS assembly could be ascribed to two reasons. One is that it could be specifically accumulated in the bacteria's negatively charged membrane due to the intensive membrane intercalation induced by the

presence of dense quaternary ammonium salt groups, and the other is that it could produce  $^1\text{O}_2$  in situ thus achieving the targeted delivery of  $^1\text{O}_2$  inside the bacteria efficiently. Moreover, this strategy is simple and practical, which avoided the complex synthesis of an antibacterial material having different antibacterial performance. Consequently, it presents a new option for the design and construction of a highly efficient antibacterial material in photodynamic therapy and holds great promise for practical applications in combatting multidrug resistant bacteria.

## EXPERIMENTAL SECTION

**Synthesis of Compound CD-QAS.** Per-6-azide-permethyl- $\beta$ -CD 6 (0.76 mmol, 1.00 g, 1.0 equiv) and 7 (3.0 mmol, 0.89 g, 10.0 equiv) were dissolved in anhydrous DMF (20 mL) and purged with nitrogen for 10 min. CuI (0.15 mmol, 0.17 g, 10.0 equiv) was subsequently added in one portion. After being purged with nitrogen for 10 min again, the reaction mixture was then refluxed under  $\text{N}_2$  atmosphere for 24 h. The insoluble copper salt was removed by filtration after cooling to room temperature, followed by adding 400 mL of acetone to get precipitation, which was filtered and washed with acetone and then recrystallized with the mixture of DMF and acetone. HPLC (reversed phase) was used to purify the crude product by using water as an eluent. A white powder was obtained in 85% yield by freeze-drying the collected fraction.  $^1\text{H}$  NMR (400 MHz,  $\text{D}_2\text{O}$ , ppm)  $\delta$  8.55 (s, 1H), 5.19 (d,  $J = 3.1$  Hz, 1H), 4.85 (s, 1H), 4.70 (d,  $J = 13.9$  Hz, 1H), 4.59 (t,  $J = 14.7$  Hz, 2H), 4.50–4.38 (m, 1H), 4.03 (t,  $J = 9.4$  Hz, 1H), 3.55 (dd,  $J = 10.0, 3.2$  Hz, 1H), 3.38 (t,  $J = 9.3$  Hz, 1H), 3.11 (s, 9H);  $^{13}\text{C}$  NMR (101 MHz,  $\text{D}_2\text{O}$ , ppm)  $\delta$  135.21 (s), 131.25 (s), 101.69 (s), 82.08 (s), 72.31 (s), 71.65 (s), 69.42 (s), 59.56 (s), 52.77 (s), 50.89 (s).

**ESR Measurement.** The  $^1\text{O}_2$  and  $\bullet\text{OH}$  generation of ruthenium compounds was detected by using TEMP and DMPO as trapping agents. In short, the ruthenium compound (0.1 mM) was exposed to white light irradiation ( $220 \text{ mW/cm}^2$ ) for 30 min with related trapping agents TEMP (1 mM). Then the signal was then observed immediately via ESR spectrometer.

**$^1\text{O}_2$  Detected by a Sensitive Probe ABDA.** ABDA was used as an  $^1\text{O}_2$ -sensitive probe to estimate the  $^1\text{O}_2$  generation ability of Ru1 and Ru2. ABDA (50  $\mu\text{M}$ ) solution was mixed with the ruthenium compounds in water (10  $\mu\text{M}$ ), and then the mixture was irradiated with  $220 \text{ mW/cm}^2$  white light. The absorbance at 378 nm of ABDA was measured at various time.  $[\text{Ru}(\text{bpy})_3]\text{Cl}_2$  ( $\Phi_{\Delta} = 0.18$  in  $\text{H}_2\text{O}$ ) was used as the standard to evaluate the  $^1\text{O}_2$  generation quantum yields for Ru1 and Ru2 under light irradiation. The  $\Phi_{\Delta}$  of different samples were calculated on the basis of the following formula:

$$\Phi_{\Delta(x)} = \Phi_{\Delta(\text{std})} \frac{K_x}{K_{\text{std}}} \frac{A_{\text{std}}}{A_x}$$

In which the subscripts x and std respectively represented the sample and  $[\text{Ru}(\text{bpy})_3]\text{Cl}_2$ .  $K$  indicated the slope of reduced absorbance at 378 nm of ABDA with irradiation time (s), where  $K_{\text{std}}$  and  $K_x$  represent the decomposition rate constants of ABDA by  $[\text{Ru}(\text{bpy})_3]\text{Cl}_2$  and Ru1 or Ru2, respectively.  $A_{\text{std}}$  and  $A_x$  were the integral areas of the absorption spectrum of  $[\text{Ru}(\text{bpy})_3]\text{Cl}_2$  and Ru1 or Ru2.

**Antimicrobial Experiments.** The microbes were first incubated with different samples, Ru1/CD-QAS ( $[\text{Ru1}] = 25 \mu\text{M}$ ,  $[\text{CD-QAS}] = 25 \mu\text{M}$ ), Ru2/CD-QAS ( $[\text{Ru2}] = 25 \mu\text{M}$ ,  $[\text{CD-QAS}] = 75 \mu\text{M}$ ), Ru1 (25  $\mu\text{M}$ ), Ru2 (25  $\mu\text{M}$ ), and -QAS (75  $\mu\text{M}$ ) for 1 h in the dark and then irradiated white light for 10 min. Then cells were spread on the separate solid culture medium agar plate. After 12 h of incubation (37  $^{\circ}\text{C}$ ) under dark, the bacteria were collected using centrifugation (4000 rpm, 5 min) and the cell death was assessed by propidium iodide (PI) staining by a confocal microscope (FV1000, Olympus, Japan).

**Confocal Laser Scanning Microscopy (CLSM) Measurements.** A total of 1.0 mL of bacterial suspension was incubated with Ru2/CD-QAS complex ( $[\text{Ru2}] = 10 \mu\text{M}$ ,  $[\text{CD-QAS}] = 30 \mu\text{M}$ )

and stained with DAPI for 15 min. The unbounded complex and excess staining reagent through centrifuging (4000 rpm, 5 min) were removed by washing the cells with PBS and the cells were resuspended in 100  $\mu$ L of PBS. Finally, the *E. coli* cells were placed on a clean glass slide and covered with a coverslip for CLSM observation.

**SEM Measurements.** A total of 1.0 mL of the bacterial suspension was treated with Ru2/CD-QAS complex ( $[Ru_2] = 25 \mu M$ ,  $[CD-QAS] = 75 \mu M$ ) the same with antibacterial experiments described above. Then the mixture was centrifuged at 4000 rpm for 5 min to remove the supernatant. *E. coli* cells were immediately placed on clean silicon slices and fixed with 2.5% glutaraldehyde in PBS. After being incubated at 4 °C overnight and washed with PBS, the cells were then dehydrated with a series of ethanol aqueous solutions for 15 min. The dehydrated cells were washed with tert-butanol and freeze-drying. Finally, the samples were plated with gold and measured by SEM.

## ■ ASSOCIATED CONTENT

### SI Supporting Information

The Supporting Information is available free of charge at <https://pubs.acs.org/doi/10.1021/acsabm.1c01018>.

<sup>1</sup>H NMR and <sup>13</sup>C NMR spectra of Ru1 and CD-QAS, high-resolution ESI mass spectrum of compound Ru1, IR spectra of products, absorption and emission spectra, UV-vis spectra change of ABDA mixed with each complex under white light irradiation, and agarose gel electrophoresis assay and cell viability toward 293T normal cells (PDF)

## ■ AUTHOR INFORMATION

### Corresponding Author

Yu Liu – Department College of Chemistry, State Key Laboratory of Elemento-Organic Chemistry, Nankai University, Tianjin 300071, China; [orcid.org/0000-0001-8723-1896](https://orcid.org/0000-0001-8723-1896); Email: [yuliu@nankai.edu.cn](mailto:yuliu@nankai.edu.cn)

### Authors

Xianyin Dai – Department College of Chemistry, State Key Laboratory of Elemento-Organic Chemistry, Nankai University, Tianjin 300071, China

Bing Zhang – Department College of Chemistry, State Key Laboratory of Elemento-Organic Chemistry, Nankai University, Tianjin 300071, China

Qilin Yu – Key Laboratory of Molecular Microbiology and Technology, College of Life Sciences, Nankai University, Tianjin 300071, China; [orcid.org/0000-0003-0473-5111](https://orcid.org/0000-0003-0473-5111)

Complete contact information is available at: <https://pubs.acs.org/doi/10.1021/acsabm.1c01018>

### Funding

This work was financially supported by the National Natural Science Foundation of China (Grant Nos. 21772099 and 21861132001).

### Notes

The authors declare no competing financial interest.

## ■ REFERENCES

- (1) Richter, M. F.; Drown, B. S.; Riley, A. P.; Garcia, A.; Shirai, T.; Svec, R. L.; Hergenrother, P. J. Predictive compound accumulation rules yield a broad-spectrum antibiotic. *Nature* **2017**, *545*, 299–304.
- (2) Alekshun, M. N.; Levy, S. B. Molecular mechanisms of antibacterial multidrug resistance. *Cell* **2007**, *128*, 1037–1050.

- (3) Garland, M.; Loscher, S.; Bogoy, M. Chemical strategies to target bacterial virulence. *Chem. Rev.* **2017**, *117*, 4422–4461.

- (4) Li, X.; Bai, H.; Yang, Y.; Yoon, J.; Wang, S.; Zhang, X. Supramolecular antibacterial materials for combatting antibiotic resistance. *Adv. Mater.* **2019**, *31*, 1805092.

- (5) Zhu, Y.; Xu, C.; Zhang, N.; Ding, X.; Yu, B.; Xu, F.-J. Polycationic Synergistic Antibacterial Agents with Multiple Functional Components for Efficient Anti-Infective Therapy. *Adv. Funct. Mater.* **2018**, *28*, 1706709.

- (6) Ding, F.; Deng, H.; Du, Y.; Shi, X.; Wang, Q. Emerging chitin and chitosan nanofibrous materials for biomedical applications. *Nanoscale* **2014**, *6*, 9477–9493.

- (7) Li, S.; Jiang, N.; Zhao, W.; Ding, Y.-F.; Zheng, Y.; Wang, L.-H.; Zheng, J.; Wang, R. eco-friendly in situ activatable antibiotic via cucurbit [8] uril-mediated supramolecular crosslinking of branched polyethylenimine. *Chem. Commun.* **2017**, *53*, 5870–5873.

- (8) Yang, Y.; Cai, Z.; Huang, Z.; Tang, X.; Zhang, X. Antimicrobial cationic polymers: From structural design to functional control. *Polym. J.* **2018**, *50*, 33–44.

- (9) Huang, Z.; Zhang, H.; Bai, H.; Bai, Y.; Wang, S.; Zhang, X. Polypseudorotaxane constructed from cationic polymer with cucurbit [7] uril for controlled antibacterial activity. *ACS Macro Lett.* **2016**, *5*, 1109–1113.

- (10) Liu, K.; Liu, Y.; Yao, Y.; Yuan, H.; Wang, S.; Wang, Z.; Zhang, X. Supramolecular photosensitizers with enhanced antibacterial efficiency. *Angew. Chem., Int. Ed.* **2013**, *52*, 8285–8289.

- (11) Bai, H.; Yuan, H.; Nie, C.; Wang, B.; Lv, F.; Liu, L.; Wang, S. A supramolecular antibiotic switch for antibacterial regulation. *Angew. Chem., Int. Ed.* **2015**, *54*, 13208–13213.

- (12) Yu, Z.-H.; Li, X.; Xu, F.; Hu, X.-L.; Yan, J.; Kwon, N.; Chen, G.-R.; Tang, T.; Dong, X.; Mai, Y.; Chen, D.; Yoon, J.; He, X.-P.; Tian, H. A Supramolecular-Based Dual-Wavelength Phototherapeutic Agent with Broad-Spectrum Antimicrobial Activity Against Drug-Resistant Bacteria. *Angew. Chem.* **2020**, *132*, 3687–3693.

- (13) Robertson, C. A.; Evans, D. H.; Abrahamse, H. Photodynamic therapy (PDT): a short review on cellular mechanisms and cancer research applications for PDT. *J. Photochem. Photobiol., B* **2009**, *96*, 1–8.

- (14) Lovell, J. F.; Liu, T. W.; Chen, J.; Zheng, G. Activatable photosensitizers for imaging and therapy. *Chem. Rev.* **2010**, *110*, 2839–2857.

- (15) Yuan, Y.; Zhang, C.-J.; Xu, S.; Liu, B. A self-reporting AIE probe with a built-in singlet oxygen sensor for targeted photodynamic ablation of cancer cells. *Chem. Sci.* **2016**, *7*, 1862–1866.

- (16) Wang, B.; Wang, M.; Mikhailovsky, A.; Wang, S.; Bazan, G. C. A membrane-intercalating conjugated oligoelectrolyte with high-efficiency photodynamic antimicrobial activity. *Angew. Chem., Int. Ed.* **2017**, *56*, 5031–5034.

- (17) Chen, J.; Gao, M.; Wang, L.; Li, S.; He, J.; Qin, A.; Ren, L.; Wang, Y.; Tang, B. Z. Aggregation-induced emission probe for study of the bactericidal mechanism of antimicrobial peptides. *ACS Appl. Mater. Interfaces* **2018**, *10*, 11436–11442.

- (18) Xiao, F.; Cao, B.; Wang, C.; Guo, X.; Li, M.; Xing, D.; Hu, X. Pathogen-specific polymeric antimicrobials with significant membrane disruption and enhanced photodynamic damage to inhibit highly opportunistic bacteria. *ACS Nano* **2019**, *13*, 1511–1525.

- (19) Wang, Y.; Feng, L.; Wang, S. Conjugated polymer nanoparticles for imaging, cell activity regulation, and therapy. *Adv. Funct. Mater.* **2019**, *29*, 1806818.

- (20) Liu, X.; Li, M.; Han, T.; Cao, B.; Qiu, Z.; Li, Y.; Li, Q.; Hu, Y.; Liu, Z.; Lam, J. W. Y.; Hu, X.; Tang, B. Z. In situ generation of azonia-containing polyelectrolytes for luminescent photopatterning and superbug killing. *J. Am. Chem. Soc.* **2019**, *141*, 11259–11268.

- (21) Ma, X.; Zhao, Y. Biomedical applications of supramolecular systems based on host–guest interactions. *Chem. Rev.* **2015**, *115*, 7794–7839.

- (22) Zhang, Y.-M.; Liu, Y.-H.; Liu, Y. Cyclodextrin-Based Multi-stimulus-Responsive Supramolecular Assemblies and Their Biological Functions. *Adv. Mater.* **2020**, *32*, 1806158.

(23) Chen, J.; Meng, Q.; Zhang, Y.; Dong, M.; Zhao, L.; Zhang, Y.; Chen, L.; Chai, Y.; Meng, Z.; Wang, C.; Jia, X.; Li, C. Complexation of an Antimicrobial Peptide by Large-Sized Macrocycles for Decreasing Hemolysis and Improving Stability. *Angew. Chem., Int. Ed.* **2021**, *60*, 11288–11293.

(24) Gao, C.; Kwong, C. H. T.; Sun, C.; Li, Z.; Lu, S.; Yang, Y.-W.; Lee, S. M. Y.; Wang, R. Selective Decoating-Induced Activation of Supramolecularly Coated Toxic Nanoparticles for Multiple Applications. *ACS Appl. Mater. Interfaces* **2020**, *12*, 25604–25615.

(25) Yan, S.; Chen, S.; Gou, X.; Yang, J.; An, J.; Jin, X.; Yang, Y. W.; Chen, L.; Gao, H. Biodegradable Supramolecular Materials Based on Cationic Polyaspartamides and Pillar [5] arene for Targeting Gram-Positive Bacteria and Mitigating Antimicrobial Resistance. *Adv. Funct. Mater.* **2019**, *29*, 1904683.

(26) Guo, S.; Huang, Q.; Chen, Y.; Wei, J.; Zheng, J.; Wang, L.; Wang, Y.; Wang, R. Synthesis and Bioactivity of Guanidinium-Functionalized Pillar[5]arene as a Biofilm Disruptor. *Angew. Chem., Int. Ed.* **2021**, *60*, 618–623.

(27) Wang, J.; Feng, L.; Yu, Q.; Chen, Y.; Liu, Y. Polysaccharide-Based Supramolecular Hydrogel for Efficiently Treating Bacterial Infection and Enhancing Wound Healing. *Biomacromolecules* **2021**, *22*, 534–539.

(28) Wei, T.; Zhan, W.; Yu, Q.; Chen, H. Smart biointerface with photoswitched functions between bactericidal activity and bacteria-releasing ability. *ACS Appl. Mater. Interfaces* **2017**, *9*, 25767–25774.

(29) Wei, T.; Tang, Z.; Yu, Q.; Chen, H. Smart antibacterial surfaces with switchable bacteria-killing and bacteria-releasing capabilities. *ACS Appl. Mater. Interfaces* **2017**, *9*, 37511–37523.

(30) Wei, T.; Zhan, W.; Cao, L.; Hu, C.; Qu, Y.; Yu, Q.; Chen, H. Multifunctional and regenerable antibacterial surfaces fabricated by a universal strategy. *ACS Appl. Mater. Interfaces* **2016**, *8*, 30048–30057.

(31) Li, X.; Lee, D.; Huang, J. D.; Yoon, J. Phthalocyanine-Assembled Nanodots as Photosensitizers for Highly Efficient Type I Photoreactions in Photodynamic Therapy. *Angew. Chem.* **2018**, *130*, 10033–10038.

(32) Dai, X.; Dong, X.; Liu, Z.; Liu, G.; Liu, Y. Controllable Singlet Oxygen Generation in Water Based on Cyclodextrin Secondary Assembly for Targeted Photodynamic Therapy. *Biomacromolecules* **2020**, *21*, 5369–5379.